Delay time calculation for dual-wavelength quantum cascade lasers

A. Hamadou, S. Lamari, Jean-Luc Thobel

Delay time calculation for dual-wavelength quantum cascade lasers

Cite as: J. Appl. Phys. **114**, 203102 (2013); https://doi.org/10.1063/1.4829914
Submitted: 16 July 2013 • Accepted: 26 October 2013 • Published Online: 25 November 2013

A. Hamadou, S. Lamari and J.-L. Thobel

Delay time calculation for dual-wavelength quantum cascade lasers

A. Hamadou,[1,2,a)] S. Lamari,[2,3] and J.-L. Thobel[4]
[1]*Département des Sciences et Techniques, Faculté des Sciences et de la Technologie, Université de Bordj Bou Arreridj 34000, Algeria*
[2]*Laboratoire d'étude des surfaces et interfaces des matériaux solides (LESIMS), Sétif 19000, Algeria*
[3]*Département de Physique, Faculté des Sciences, Université Sétif 1, 19000, Algeria*
[4]*Institut d'Electronique, de Microélectronique et de Nanotechnologie (IEMN), UMR 8520, Université Lille1, Avenue Poincaré, BP 60069, 59652 Villeneuve d'Ascq Cédex, France*

(Received 16 July 2013; accepted 26 October 2013; published online 25 November 2013)

In this paper, we calculate the turn-on delay (t_{th}) and buildup (Δt) times of a midinfrared quantum cascade laser operating simultaneously on two laser lines having a common upper level. The approach is based on the four-level rate equations model describing the variation of the electron number in the states and the photon number present within the cavity. We obtain simple analytical formulae for the turn-on delay and buildup times that determine the delay times and numerically apply our results to both the single and bimode states of a quantum cascade laser, in addition the effects of current injection on t_{th} and Δt are explored. © *2013 AIP Publishing LLC*.
[http://dx.doi.org/10.1063/1.4829914]

I. INTRODUCTION

Simultaneous multi-wavelength operation of a quantum cascade (QC) laser[1] in the mid-infrared range has attracted much attention in recent years mainly due to potential applications in areas such as sensing of trace-gases through an analysis based on differential absorption light detection and ranging (LIDAR).[2] Another possible application is the nonlinear mixing of two wavelengths to generate light at a third one, for instance, terahertz radiation has been obtained by difference frequency generation from two mid-infrared modes by the authors of Refs. 3–5.

Up until now, various operating schemes for the multi-wavelength QC laser have been put forward by different authors. Among the notable designs, the following can be mentioned: Two consecutive optical transitions between three energy levels,[6] multiple-wavelength superlattice QC laser,[7] QC laser with alternative design approach containing five different material composition,[8] QC laser with two substacks region,[9–11] and QC laser with high k-space lasing.[12]

In a QC laser, the delay time plays an important role that partly determines the device's performance and has already been investigated theoretically in the case of a single mode system.[13,14] For single mode QC lasers, the strong decrease of the delay time with current was then attributed to the dependence of the turn-on delay and buildup times on current injection.

The dynamics of multimode QC lasers is much more complex than that of single mode ones because of the modes' competition for gain. As a case in point, in Ref. 15, we showed on the basis of numerical calculations that for a dual-wavelength QC laser the respective numbers of photons for the two modes compete before the stationary regime is reached, the total photon number in the cavity remaining constant throughout.

The aim of this paper is to present a theoretical analysis that accounts for the dynamics of a multi-wavelength mid-infrared QC laser. Our approach is simple and intuitive and based on the rate equations model. Our focus will only be on the special case of a two-wavelength laser where the transitions share the same upper level and therefore compete against each other for gain. Moreover, optical nonlinearities are ignored and the two modes are therefore uncoupled.

Our paper is organized as follows: Section I is a general introduction to the subject while Sec. II describes the rate equations model of the two modes used to derive our results. Section III contains an analytical derivation of the turn-on delay and buildup times for both the single and bimode states. Finally, Sec. IV concludes our paper and highlights our main findings.

II. RATE EQUATIONS OF A DUAL-WAVELENGTH QC LASER

A. The structure

Our investigation will focus on a four-level QC laser operating simultaneously on two laser lines having a common upper level. Fig. 1 shows the energy-level diagram of one stage of the active region in such as system. The upper and lower states for wavelength λ_1 will be taken as levels 4 and 3, respectively, while 4 and 2 will be for λ_2. For mode 1 of wavelength λ_1, the first excited state denoted 2 and the ground state denoted 1 are used to empty the lower state through emission of longitudinal optical (LO) phonons. The same ground state, through LO-phonon emission, is also used to empty the lower state of the lasing mode 2 at wavelength λ_2. We note in passing that intersubband phonon scattering also occurs between levels 4 and 1, 4 and 2 on one hand, and 4 and 3 on the other and it has been shown to be the main competing non-radiative process in mid-infrared QC lasers.[10]

An example of such a structure is the laser realized by the authors of Ref. 10, which consists of two stacks of stages.

[a)]Author to whom correspondence should be addressed. Electronic mail: abd_hamado@yahoo.fr

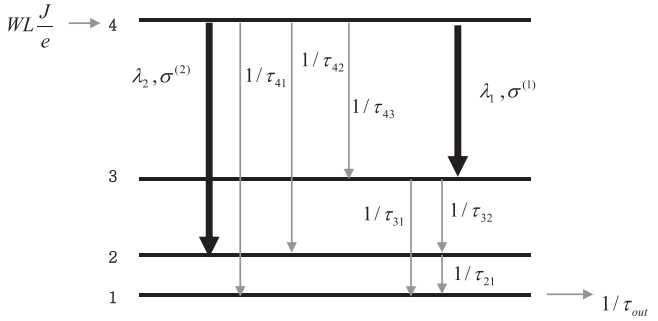

FIG. 1. Four-level-model system of the bound-to-continuum stage in a dual-wavelength QC laser as used in our work. Lasing takes place simultaneously through transitions from 4 onto 3 on one hand and from 4 onto 2 on the other.

In the first stack, a double phonon resonance design is in action[16–18] and lasing takes place around a wavelength λ_1 at 10.5 μm. On the other hand, the second stack uses a bound-to-continuum design[18,19] with lasing occurring at a wavelength λ_2 about 8.9 μm. For more technical details on the structure, we kindly refer the reader to the published literature.[3,10] In intersubband transitions, the lifetimes of the energy levels are mostly determined by the non-radiative scattering mechanisms such as LO-phonon, acoustic phonon, electron–electron, interface roughness, and impurity scattering processes.[20] In the mid-infrared, it is well known that the LO-phonon scattering is the dominant process.[21]

B. The rate equations model

Denote by N_1, N_2, N_3, and N_4 the respective instantaneous numbers of electrons in each of the four levels and by $S^{(1)}$ and $S^{(2)}$ the photon numbers for modes 1 of wavelength λ_1 and 2 of wavelength λ_2, respectively. Neglecting optical nonlinearities for the moment, the two modes decouple in the electromagnetic sense and the system may then be described by the six following rate equations:[15]

$$\frac{dN_4}{dt} = WL\frac{J}{e} - \frac{N_4}{\tau_4} - \Gamma^{(1)}\frac{c'\sigma^{(1)}}{V}(N_4 - N_3)S^{(1)} - \Gamma^{(2)}\frac{c'\sigma^{(2)}}{V}(N_4 - N_2)S^{(2)}, \quad (1a)$$

$$\frac{dN_3}{dt} = \frac{N_4}{\tau_{43}} - \frac{N_3}{\tau_3} + \Gamma^{(1)}\frac{c'\sigma^{(1)}}{V}(N_4 - N_3)S^{(1)}, \quad (1b)$$

$$\frac{dN_2}{dt} = \frac{N_4}{\tau_{42}} + \frac{N_3}{\tau_{32}} - \frac{N_2}{\tau_{21}} + \Gamma^{(2)}\frac{c'\sigma^{(2)}}{V}(N_4 - N_2)S^{(2)}, \quad (1c)$$

$$\frac{dN_1}{dt} = \frac{N_4}{\tau_{41}} + \frac{N_3}{\tau_{31}} + \frac{N_2}{\tau_{21}} - \frac{N_1}{\tau_{out}}, \quad (1d)$$

$$\frac{dS^{(1)}}{dt} = N_p\Gamma^{(1)}\frac{c'\sigma^{(1)}}{V}(N_4 - N_3)S^{(1)} - \frac{S^{(1)}}{\tau_p^{(1)}} + N_p\beta^{(1)}\frac{N_4}{\tau_{sp}^{(1)}}, \quad (1e)$$

$$\frac{dS^{(2)}}{dt} = N_p\Gamma^{(2)}\frac{c'\sigma^{(2)}}{V}(N_4 - N_2)S^{(2)} - \frac{S^{(2)}}{\tau_p^{(2)}} + N_p\beta^{(2)}\frac{N_4}{\tau_{sp}^{(2)}}. \quad (1f)$$

In the above system of equations, J denotes the electron current density that is pumped into the upper level and e is the absolute value of the electronic charge, while W and L are the lateral dimensions of the cavity. Denoting by N_p and L_p the number of stages and length of each one of these, the whole volume V of the active area is then given by N_pWLL_p. In addition, in the above equations, we introduced the mode confinement factors $\Gamma^{(i)}$ for wavelengths λ_i (i =1,2), and the average velocity of light in the system c' given by $c' = c/n_{eff}$ where c and n_{eff} are, respectively, the speed of light in vacuum and the effective refractive index of the cavity. In our case, we ignore the difference between the effective refractive indices of the two modes. The important parameters $\beta^{(i)}$ in Eqs. (1e) and (1f) define the respective proportions of spontaneous emission when a photon is emitted into the corresponding cavity mode.[22] On the other hand, $\sigma^{(i)}$ stands for the stimulated emission cross section for the transition corresponding to wavelengths λ_i. The system dynamics is mainly determined by the six non radiative scattering times denoted by τ_{43}, τ_{42}, τ_{41}, τ_{32}, τ_{31}, and τ_{21} that are due to LO-phonon emission and radiative spontaneous relaxation times $\tau_{sp}^{(i)}$ for the two transitions involved. Furthermore, between two adjacent stages we model the escape of electrons by a rate $1/\tau_{out}$, where τ_{out} stands for the electrons escape time.[23] To complete the picture, we take into consideration for both modes the finite lifetimes of the photons denoted by $\tau_p^{(i)}$. For the sake of convenience, let us also introduce the lifetimes τ_4 and τ_3 of the levels 4 and 3, which we write as $\tau_4 = 1/(1/\tau_{43} + 1/\tau_{42} + 1/\tau_{41})$ and $\tau_3 = 1/(1/\tau_{32} + 1/\tau_{31})$.

The radiative spontaneous emission relaxation times for both transitions can be cast as follows:[24]

$$\frac{1}{\tau_{sp}^{(i)}} = \frac{8\pi^2 n_{eff}\left(ez^{(i)}\right)^2}{\varepsilon_0\hbar\lambda_i^3}, \quad \text{i=1,2}, \quad (2)$$

where $ez^{(i)}$ is the dipole matrix element of the transition in question while ε_0 and $\hbar$ have their usual meaning.

In the steady state, all the time derivatives in the rate equations given above vanish, the normalized intersubband population inversions $\Delta\tilde{N}^{(1)}$ and $\Delta\tilde{N}^{(2)}$ as functions of the normalized photon numbers $\tilde{S}^{(1)}$ and $\tilde{S}^{(2)}$ can then be written as[15]

$$\Delta\tilde{N}^{(i)} = \frac{p^{(i)}\left(1 + \delta_i\tilde{S}^{(j)}\right)}{1 + \tilde{S}^{(1)} + \tilde{S}^{(2)} + \theta\tilde{S}^{(1)}\tilde{S}^{(2)}} \quad i,j = 1,\,2,\,(i \neq j), \quad (3)$$

where

$$\delta_1 = \frac{1}{\left(\frac{\tau_4}{\tau_{21}} + \frac{\tau_4\tau_3}{\tau_{43}\tau_{31}} + \frac{\tau_4}{\tau_{41}}\right)}, \quad (4a)$$

$$\delta_2 = \frac{\tau_3\left(1 - \frac{\tau_{21}}{\tau_{32}} - \frac{\tau_{21}}{\tau_{42}}\right)}{\tau_4\left(1 - \frac{\tau_3\tau_{21}}{\tau_{43}\tau_{32}} - \frac{\tau_{21}}{\tau_{42}}\right)\left(1 + \frac{\tau_3}{\tau_{42}} + \frac{\tau_3}{\tau_{41}}\right)}, \quad (4b)$$

$$\theta = \frac{\frac{\tau_3}{\tau_4}\left(1 + \frac{\tau_{21}}{\tau_{31}} + \frac{\tau_{21}}{\tau_{41}}\right)}{\left(1 + \frac{\tau_3}{\tau_{42}} + \frac{\tau_3}{\tau_{41}}\right)\left(1 + \frac{\tau_3\tau_{21}}{\tau_{43}\tau_{31}} + \frac{\tau_{21}}{\tau_{41}}\right)}, \quad (4c)$$

$$p^{(i)} = \frac{J}{J_{th}^{(i)}}, \quad \Delta\tilde{N}^{(i)} = \frac{\Delta N^{(i)}}{\Delta N_{th}^{(i)}}, \quad \tilde{S}^{(i)} = \frac{S^{(i)}}{S_{sat}^{(i)}}, \quad i = 1, 2 \tag{4d}$$

where the intersubband threshold population inversions in total absence of photons $\Delta N_{th}^{(1)}$ and $\Delta N_{th}^{(2)}$ and the photon saturation numbers for both modes are defined as[15]

$$\Delta N_{th}^{(1)} = WL\frac{J_{th}^{(1)}}{e}\tau_4\left(1 - \frac{\tau_3}{\tau_{43}}\right), \tag{5a}$$

$$\Delta N_{th}^{(2)} = WL\frac{J_{th}^{(2)}}{e}\tau_4\left(1 - \frac{\tau_3\tau_{21}}{\tau_{43}\tau_{32}} - \frac{\tau_{21}}{\tau_{42}}\right), \tag{5b}$$

$$S_{sat}^{(1)} = \frac{1}{\tau_4\left(1 + \frac{\tau_3}{\tau_{42}} + \frac{\tau_3}{\tau_{41}}\right)\Gamma^{(1)}\frac{c'\sigma^{(1)}}{V}}, \tag{5c}$$

$$S_{sat}^{(2)} = \frac{1}{\tau_4\left(1 + \frac{\tau_3\tau_{21}}{\tau_{43}\tau_{31}} + \frac{\tau_{21}}{\tau_{41}}\right)\Gamma^{(2)}\frac{c'\sigma^{(2)}}{V}}. \tag{5d}$$

In Eqs. (5a) and (5b), the threshold current density $J_{th}^{(1)}$ and $J_{th}^{(2)}$ are expressed as[15]

$$\frac{J_{th}^{(1)}}{e} = \frac{L_p}{\Gamma^{(1)}c'\sigma^{(1)}\tau_4\tau_p^{(1)}}\frac{1}{\left(1 - \frac{\tau_3}{\tau_{43}}\right)}, \tag{6a}$$

$$\frac{J_{th}^{(2)}}{e} = \frac{L_p}{\Gamma^{(2)}c'\sigma^{(2)}\tau_4\tau_p^{(2)}}\frac{1}{\left(1 - \frac{\tau_3\tau_{21}}{\tau_{43}\tau_{32}} - \frac{\tau_{21}}{\tau_{42}}\right)}. \tag{6b}$$

Note that the expression for $J_{th}^{(2)}$ given by Eq. (6b) is the threshold current density in absence of any optical field in the cavity and is to be distinguished from the physical threshold $\tilde{J}_{th}^{(2)}$; both these currents are however related to one another by[15] $\tilde{J}_{th}^{(2)} = \left(1 + \frac{1}{\delta_2}\left(\frac{J_{th}^{(2)}}{J_{th}^{(1)}} - 1\right)\right)J_{th}^{(1)}$.

We note in passing that the threshold current density for wavelength λ_1 is lower than that for wavelength λ_2.[10]

The only non trivial stable photon numbers can then be obtained as[15]

(i) single mode state

$$S^{(1)} = S_{sat}^{(1)}(p^{(1)} - 1), \tag{7a}$$

$$S^{(2)} = 0, \tag{7b}$$

for

$$1\langle p^{(1)}\langle 1 + \frac{1}{\delta_2}\left(\frac{J_{th}^{(2)}}{J_{th}^{(1)}} - 1\right) = p_{2,th}^{(1)}, \tag{8}$$

(ii) bimode state

$$S^{(1)} = S_{sat}^{(1)}\frac{-a_1 + \left(a_1^2 - 4a_0\right)^{1/2}}{2}, \tag{9a}$$

$$S^{(2)} = S_{sat}^{(2)}\frac{p^{(2)} - 1 + \left(p^{(2)}\delta_2 - 1\right)\tilde{S}^{(1)}}{1 + \theta\tilde{S}^{(1)}}, \tag{9b}$$

for

$$p^{(1)}\rangle p_{2,th}^{(1)}, \tag{9c}$$

where

$$a_1 = \left(\frac{\delta_1}{\delta_2\theta} - \frac{1}{\delta_2}\right)\frac{J_{th}^{(2)}}{J_{th}^{(1)}} + \frac{1}{\delta_2} + \frac{1}{\theta} - p^{(1)}\frac{\delta_1}{\theta}, \tag{10a}$$

$$a_0 = -\frac{(1 - \delta_1)}{\delta_2\theta}\frac{J_{th}^{(2)}}{J_{th}^{(1)}} + \frac{1}{\delta_2\theta} - p^{(1)}\frac{\delta_1}{\delta_2\theta}, \tag{10b}$$

and

$$p^{(2)} = \frac{J_{th}^{(1)}}{J_{th}^{(2)}}p^{(1)}. \tag{10c}$$

It is important to note that the quantity $p_{2,th}^{(1)}$ displayed in Eq. (8) is actually the physical threshold current density normalized by the threshold current density for mode 1, i.e., $\tilde{J}_{th}^{(2)}/J_{th}^{(1)}$ and is known as the second QC laser threshold.

Next using the theory developed above, we estimate numerically $\tau_{sp}^{(1)}$, $\tau_{sp}^{(2)}$, $J_{th}^{(2)}/J_{th}^{(1)}$, $p_{2,th}^{(1)}$, and for the single mode state compute $\tilde{S}^{(1)}$ while for the bimode state we compute $\tilde{S}^{(1)}$ and $\tilde{S}^{(2)}$ for two pumping strengths $p^{(1)} = 1.45$ and $p^{(1)} = 2.5$. Our computation use the following calculated QC laser parameters at room temperature as reported in Refs. 10, 15, and 22: $\tau_4 = 1$ ps, $\tau_{43} = 12.5$ ps, $\tau_{42} = 2.3$ ps, $\tau_{41} = 2.1$ ps, $\tau_3 = 0.13$ ps, $\tau_{32} = 3$ ps, $\tau_{31} = 0.15$ ps, $\tau_{21} = 0.18$ ps, $n_{eff} = 3.27$, $\beta^{(1)} = \beta^{(2)} = 2 \times 10^{-3}$, $z^{(1)} = 1.57$ nm, and $z^{(2)} = 1.8$ nm. Our results are as follows: $\tau_{sp}^{(1)} = 66$ ns, $\tau_{sp}^{(2)} = 30$ ns, $J_{th}^{(2)}/J_{th}^{(1)} \approx 1.06$, $p_{2,th}^{(1)} = 1.55$, $\tilde{S}^{(1)} = 0.45$ for the single mode state, and $\tilde{S}^{(1)} = 1.17$ and $\tilde{S}^{(2)} = 0.38$ for the bimode one.

III. DERIVATION OF THE TURN-ON DELAY AND BUILDUP TIMES

To compute the delay time t_d that elapses between the moment the bias is applied and the time the photon number reaches 10% of its stationary value we write $t_d = t_{th} + \Delta t$, where t_{th} is the turn-on delay time needed for the population inversion ΔN to reach its threshold value ΔN_{th} while Δt is the buildup time. During this interval of time Δt, the number of photons is growing but is still very small, so that we may assume that the population inversion remains constant.

In order to get the explicit turn-on delay time equation for a dual-wavelength QC laser, it is convenient to determine the population inversion in terms of the QC laser parameters in the total absence of photons. We first derive the turn-on delay time for wavelength λ_1 and follow with that of wavelength λ_2, we then derive the buildup times for wavelengths

λ_1 and λ_2, respectively. Our results are applied on the two modes of QC laser: Single mode and bimode states.

A. Turn-on delay time for wavelength λ_1

Using the same procedure as that used in Ref. 13, we can compute the turn-on delay time $t_{th}^{(1)}$ for wavelength λ_1.

With the initial condition $N_4(t=0)=0$, Eq. (1a) can directly be solved yielding

$$N_4(t) = WL\frac{J}{e}\tau_4\left(1-e^{-\frac{t}{\tau_4}}\right). \tag{11}$$

For $N_3(t)$, we use Eq. (1b) and write the solution as

$$N_3(t) = u(t)v(t). \tag{12}$$

Substituting Eq. (12) back into Eq. (1b) in the absence of any light fields and differentiating, we get

$$u(t)\left(\frac{dv(t)}{dt}+\frac{v}{\tau_3}\right)+v(t)\frac{du(t)}{dt}=\frac{N_4}{\tau_{43}}. \tag{13}$$

The solution being unique, we first get rid of the first term in Eq. (13) by choosing v(t) as

$$v(t) = e^{-\frac{t}{\tau_3}}, \tag{14}$$

and then the remaining terms are easily handled and give for $u(t)$ the following expression:

$$u(t) = WL\frac{J}{e}\frac{\tau_4}{\tau_{43}}\left(\tau_3 e^{\frac{t}{\tau_3}}+\frac{1}{\frac{1}{\tau_4}-\frac{1}{\tau_3}}e^{-\left(\frac{1}{\tau_4}-\frac{1}{\tau_3}\right)t}\right)+WL\frac{J}{e}\frac{\tau_4}{\tau_{43}}c_1, \tag{15}$$

where c_1 is a constant to be determined below by the initial conditions.

Combining Eqs. (12), (14), and (15), we get the following expression for N_3:

$$N_3(t)=WL\frac{J}{e}\tau_4\left(\frac{1}{\tau_{43}}\left(\tau_3+\frac{1}{\frac{1}{\tau_4}-\frac{1}{\tau_3}}e^{-\frac{t}{\tau_4}}\right)+\frac{1}{\tau_{43}}c_1e^{-\frac{t}{\tau_3}}\right). \tag{16}$$

The initial condition $N_3(t=0)=0$ is fulfilled if we set $c_1=-\left(\tau_3+\frac{1}{\frac{1}{\tau_4}-\frac{1}{\tau_3}}\right)$ and the solution then becomes

$$N_3(t) = WL\frac{J}{e}\frac{\tau_4\tau_3}{\tau_{43}}\left[\frac{\frac{\tau_3}{\tau_4}\left(1-e^{-\frac{t}{\tau_3}}\right)-1+e^{-\frac{t}{\tau_4}}}{\frac{\tau_3}{\tau_4}-1}\right]. \tag{17}$$

From Eqs. (11) and (17) we deduce the population inversion between levels 4 and 3 for the single mode at wavelength λ_1 as:

$$\Delta N^{(1)}(t)=WL\frac{J}{e}\tau_4\left(1-e^{-\frac{t}{\tau_4}}\right)\xi_1-WL\frac{J}{e}\tau_4\left(1-e^{-\frac{t}{\tau_3}}\right)\xi_2, \tag{18}$$

where the coefficients ξ_1 and ξ_2 are defined as

$$\xi_1 = 1+\frac{\tau_3}{\tau_{43}}\frac{1}{\frac{\tau_3}{\tau_4}-1}, \tag{19a}$$

$$\xi_2 = -\frac{\tau_3}{\tau_{43}}\frac{\tau_3}{\tau_4}\frac{1}{\frac{\tau_3}{\tau_4}-1}. \tag{19b}$$

The threshold condition $\Delta N^{(1)}=\Delta N_{th}^{(1)}$ is reached after a time $t_{th}^{(1)}$ solution of the equation that results by combining Eqs. (5a), (6a), and (18), i.e.,

$$\frac{\xi_1\exp\left(-\frac{t_{th}^{(1)}}{\tau_4}\right)+\xi_2\exp\left(-\frac{t_{th}^{(1)}}{\tau_3}\right)}{\xi_1+\xi_2}=1-\frac{1}{p^{(1)}}. \tag{20}$$

Note that Eq. (20) is valid for any value of $p^{(1)}$.

B. Turn-on delay time for wavelength λ_2

Using the same procedure as for wavelength λ_1, we can now compute the turn-on delay time $t_{th}^{(2)}$ for wavelength λ_2.

Let us introduce for convenience the function $h(t)$ given by

$$h(t)=\frac{N_4(t)}{\tau_{42}}+\frac{N_3(t)}{\tau_{32}}. \tag{21}$$

Using Eqs. (11) and (17) for N_4 and N_3, we have

$$h(t)=WL\frac{J}{e}\tau_4\left[\xi_3\left(1-e^{-\frac{t}{\tau_4}}\right)+\xi_4\left(1-e^{-t/\tau_3}\right)\right], \tag{22}$$

where

$$\xi_3 = \frac{1}{\tau_{42}}-\frac{1}{\tau_{43}}\frac{\tau_3}{\tau_{32}}\frac{1}{\frac{\tau_3}{\tau_4}-1}, \tag{23a}$$

$$\xi_4 = \frac{1}{\tau_{43}}\frac{\tau_3}{\tau_{32}}\frac{\tau_3}{\tau_4}\frac{1}{\frac{\tau_3}{\tau_4}-1}. \tag{23b}$$

Then, Eq. (1c) becomes

$$\frac{dN_2(t)}{dt}=h(t)-\frac{N_2(t)}{\tau_{21}}. \tag{24}$$

Using the same procedure as that used for the wavelength λ_1, we get the following expression for N_2:

$$N_2(t)=WL\frac{J}{e}\tau_4\left[(\xi_3+\xi_4)\tau_{21}-\frac{\xi_3e^{-\frac{t}{\tau_4}}}{\frac{1}{\tau_{21}}-\frac{1}{\tau_4}}-\frac{\xi_4e^{-\frac{t}{\tau_3}}}{\frac{1}{\tau_{21}}-\frac{1}{\tau_3}}-\left((\xi_3+\xi_4)\tau_{21}-\frac{\xi_3}{\frac{1}{\tau_{21}}-\frac{1}{\tau_4}}-\frac{\xi_4}{\frac{1}{\tau_{21}}-\frac{1}{\tau_3}}\right)e^{-\frac{t}{\tau_{21}}}\right]. \tag{25}$$

From Eqs. (11) and (25), we deduce the population inversion $\Delta N^{(2)}$ for wavelength λ_2 between levels 4 and 2 as

$$\Delta N^{(2)} = WL\frac{J}{e}\tau_4\left[1-(\xi_3+\xi_4)\tau_{21}+\Lambda_1 e^{-\frac{t}{\tau_4}}+\Lambda_2 e^{-\frac{t}{\tau_3}}+\Lambda_3 e^{-\frac{t}{\tau_{21}}}\right], \tag{26}$$

where the coefficients Λ_1, Λ_2, and Λ_3 are defined through

$$\Lambda_1 = \frac{\xi_3}{\left(\frac{1}{\tau_{21}}-\frac{1}{\tau_4}\right)} - 1, \tag{27a}$$

$$\Lambda_2 = \frac{\xi_4}{\left(\frac{1}{\tau_{21}}-\frac{1}{\tau_3}\right)}, \tag{27b}$$

$$\Lambda_3 = (\xi_3+\xi_4)\tau_{21} - \frac{\xi_3}{\left(\frac{1}{\tau_{21}}-\frac{1}{\tau_4}\right)} - \frac{\xi_4}{\left(\frac{1}{\tau_{21}}-\frac{1}{\tau_3}\right)}. \tag{27c}$$

The threshold condition $\Delta N^{(2)} = \Delta N_{th}^{(2)}$ is reached after a time $t_{th}^{(2)}$ solution of the following equation that results by combining Eqs. (5b), (6b), and (26), i.e.:

$$\frac{\Lambda_1 \exp\left(-\frac{t_{th}^{(2)}}{\tau_4}\right)+\Lambda_2 \exp\left(-\frac{t_{th}^{(2)}}{\tau_3}\right)+\Lambda_3 \exp\left(-\frac{t_{th}^{(2)}}{\tau_{21}}\right)}{\Lambda_1+\Lambda_2+\Lambda_3} = 1-\frac{1}{p^{(2)}}. \tag{28}$$

Figure 2 shows the turn-on delay time as a function of normalized current injection $p^{(1)}$, which we vary in the interval $[1, p_{2,th}^{(1)}]$. When the current injection is close to the first threshold ($p^{(1)} \approx 1$), the turn-on delay time is high, which means that the laser is slow in reaching its operating regime; in contrast, the situation reverses when current injection is significantly above the threshold.

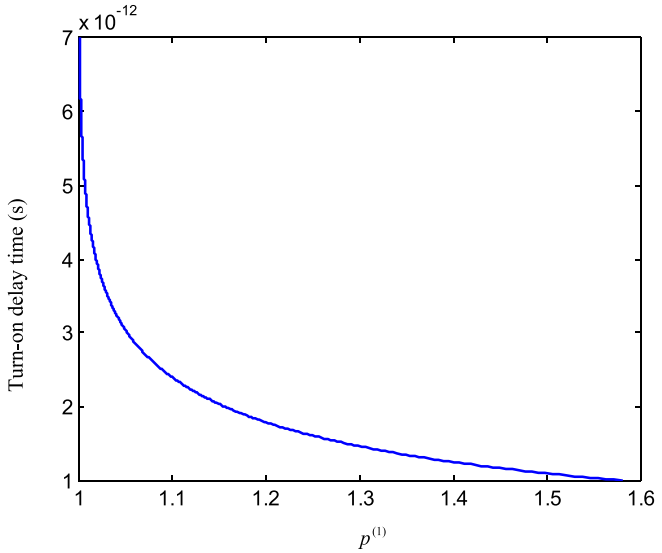

FIG. 2. Turn-on delay time $t_{th}^{(1)}$ variation for the single mode state of wavelength λ_1 as a function of the normalized current density $p^{(1)}$ for $1\langle p^{(1)}\langle p_{2,th}^{(1)}$.

In Fig 3, we show the variation of the turn-on delay times for the bimode state of the QC laser as a function of the normalized current density which we vary from the second QC laser threshold $p_{2,th}^{(1)}$ to 7 i.e., $p_{2,th}^{(1)}\langle p^{(1)}\langle 7$. The blue solid line and red dashed one are for modes at wavelengths λ_1 and λ_2, respectively. It is worthwhile to stress the strong decrease of t_{th} as the injected current increases from its minimal value upward. In addition, far from the second QC laser threshold, for both modes the turn-on delay times are very close.

C. Buildup time for wavelength λ_1 and λ_2

In order to determine the evolution of the photon number in the time interval where the oscillation of population inversion develops linearly, one can replace the dynamic variables $\Delta N^{(i)}$ $(i=1,2)$ and N_4 by their respective values $\Delta N_0^{(i)}$ $(i=1,2)$ and $N_{4,0}$ when the number of photons in the cavity is still very small,[15] and retains the equations which results from it for the $S^{(i)}$ $(i=1,2)$ variables only.

From Eqs. (1a), (3), and (5), we obtain for $N_{4,0}$, $\Delta N_0^{(1)}$, and $\Delta N_0^{(2)}$

$$N_{4,0} = WL\frac{J}{e}\tau_4, \tag{29a}$$

$$\Delta N_0^{(1)} = WL\frac{J}{e}\tau_4\left(1-\frac{\tau_3}{\tau_{43}}\right), \tag{29b}$$

$$\Delta N_0^{(2)} = WL\frac{J}{e}\tau_4\left(1-\frac{\tau_3\tau_{21}}{\tau_{43}\tau_{32}}-\frac{\tau_{21}}{\tau_{42}}\right). \tag{29c}$$

Substituting these into Eq. (1e) and taking into account Eq. (5), we obtain the following linear first order differential equation for the photon number for wavelength λ_1:

$$\frac{dS^{(1)}}{dt} = \frac{1}{\tau_p^{(1)}}(p^{(1)}-1)S^{(1)} + WL\frac{J}{e}\tau_4\frac{N_p\beta^{(1)}}{\tau_{sp}^{(1)}}. \tag{30}$$

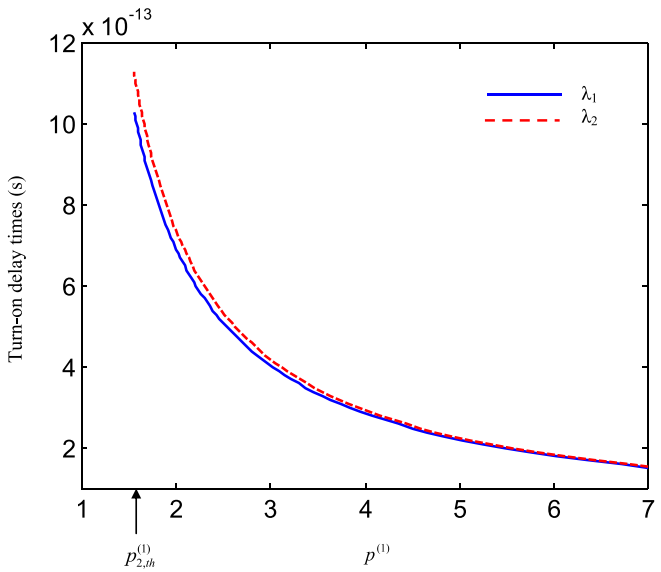

FIG. 3. Variation of the turn-on delay times $t_{th}^{(1)}$ and $t_{th}^{(2)}$ for the bimode state as a function of normalized current density $p^{(1)}$ in the interval $p_{2,th}^{(1)}\langle p^{(1)}\langle 7$, blue solid line and red dashed one are for modes 1 and 2, respectively.

We use the following initial conditions for the intra-cavity photon number $S^{(1)} = 0$. Then, Eq. (30) can be directly solved; thus,

$$S^{(1)}(t) = \frac{\tau_p^{(1)}}{\left(p^{(1)} - 1\right)} WL \frac{J}{e} \tau_4 \frac{N_p \beta^{(1)}}{\tau_{sp}^{(1)}} \left(e^{\left(p^{(1)}-1\right)\frac{t}{\tau_p^{(1)}}} - 1 \right). \quad (31)$$

Now, to compute the buildup time $\Delta t_{10\%}$, i.e., the time necessary for the laser to reach 10% of its stationary photon number, we invert Eq. (31) to get for the single mode state

$$\Delta t_{10\%} = \frac{\tau_p^{(1)}}{p^{(1)} - 1} \ln \left(1 + \frac{1}{10} \frac{\left(p^{(1)} - 1\right)^2}{p^{(1)}} \frac{\tau_{sp}^{(1)}}{\beta^{(1)}} \frac{\left(1 - \frac{\tau_3}{\tau_{43}}\right)}{\tau_4 \left(1 + \frac{\tau_3}{\tau_{42}} + \frac{\tau_3}{\tau_{41}}\right)} \right). \quad (32)$$

Using the same procedure as that used above, we can compute the buildup time for wavelengths bimode state at λ_1 and λ_2, respectively,

$$\Delta t_{10\%}^{(1)} = \frac{\tau_p^{(1)}}{p^{(1)} - 1} \ln \left(1 + \frac{1}{10} \left(\frac{p^{(1)} - 1}{p^{(1)}} \right) \tilde{S}^{(1)} \frac{\tau_{sp}^{(1)}}{\beta^{(1)}} \frac{\left(1 - \frac{\tau_3}{\tau_{43}}\right)}{\tau_4 \left(1 + \frac{\tau_3}{\tau_{42}} + \frac{\tau_3}{\tau_{41}}\right)} \right), \quad (33)$$

$$\Delta t_{10\%}^{(2)} = \frac{\tau_p^{(2)}}{p^{(2)} - 1} \ln \left(1 + \frac{1}{10} \left(\frac{p^{(2)} - 1}{p^{(2)}} \right) \tilde{S}^{(2)} \frac{\tau_{sp}^{(2)}}{\beta^{(2)}} \frac{\left(1 - \frac{\tau_3 \tau_{21}}{\tau_{43} \tau_{32}} - \frac{\tau_{21}}{\tau_{42}}\right)}{\tau_4 \left(1 + \frac{\tau_3 \tau_{21}}{\tau_{43} \tau_{31}} + \frac{\tau_{21}}{\tau_{41}}\right)} \right). \quad (34)$$

In Fig. 4, the buildup time for the single mode state is plotted versus normalized current injection, which we vary from the first QC laser threshold $p^{(1)} = 1$ to $p^{(1)} = p_{2,th}^{(1)}$. We find that the buildup time is almost inversely proportional to the normalized current density.

In Fig 5, we show the variation of the buildup times for the bimode state as a function of the normalized current density which we vary from the second QC laser threshold $p^{(1)} = p_{2,th}^{(1)}$ to $p^{(1)} = 6$. The blue solid line and red dashed one are for modes 1 and 2, respectively. When the current injection is close to the second QC laser threshold, the buildup time for wavelength λ_1 is large meaning that mode 1 is slow whereas for wavelength λ_2 the buildup time increases quickly meaning that the onset of mode 2 is fast but then becomes slow. When the current injection is significantly above the second QC laser threshold, the buildup times for both modes are small, which mean that both modes are fast.

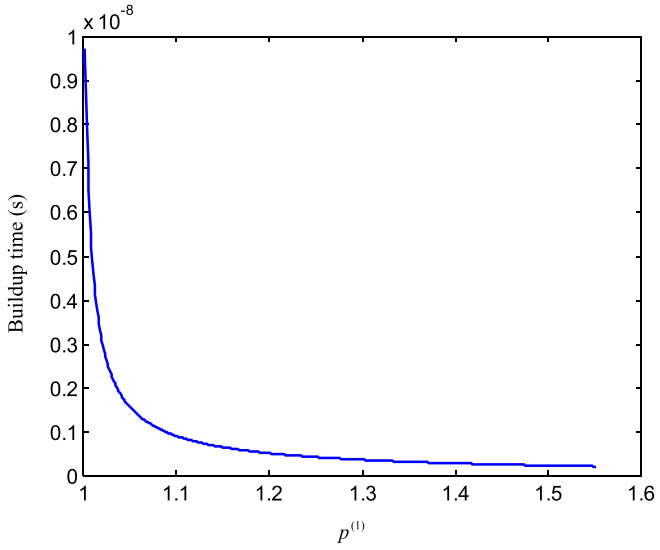

FIG. 4. Buildup time variation for the single mode state as a function of normalized current density for $1\langle p^{(1)} \langle p_{2,th}^{(1)}$ and for $\tau_p^{(1)} = 9.5$ ps.

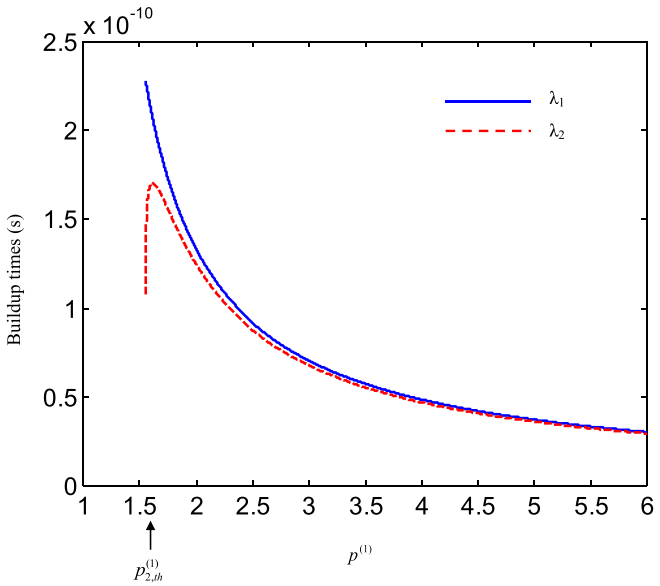

FIG. 5. Variation of the buildup times for the bimode state as a function of the normalized current density $p^{(1)}$for $p^{(1)}\rangle p_{2,th}^{(1)}$. Blue solid line and red dashed one are for modes 1 and 2, respectively, and for $\tau_p^{(1)} = 9.5$ ps and $\tau_p^{(2)} = 9.3$ ps.

In addition, far from threshold, the buildup times for both wavelengths are very close. Moreover, the rates of decay for wavelengths λ_1 and λ_2 depend on the dual-wavelength QC laser parameters.

The derivation of our results assumes the different relaxation times entering our rate equations to be independent of the injected current density J.

While this is a very reasonable assumption, it would be an interesting question to explore to see what happens when the current J is very strong or is time dependent.

IV. CONCLUSION

Using a simple and intuitive rate equations model, we developed an analytical scheme to derive the dynamical characteristics such as turn-on delay and buildup times as functions of current and the different scattering times of the system of a dual-wavelength midinfrared QC laser. First, for the single mode state, we find as expected that the turn-on delay time decreases from as high a value as 7 ps at threshold to as low as 1.12 ps as we sweep the injection current from $J_{th}^{(1)}$ to $1.55\,J_{th}^{(1)}$. As we increase the injection current further we reach the second threshold at $1.55\,J_{th}^{(1)}$, beyond which the system switches to the bimode state. For values of the injection current $1.55 \leq J/J_{th}^{(1)} \leq 1.59$ the turn-on delay times for both modes are in the picosecond range but as the current is increased further this parameter falls in the sub-picosecond ball park.

As for the buildup time, in the single mode state this important parameter decreases with current strength from a high value of 10 nanoseconds (ns) at threshold to 0.23 ns for $J = 1.55J_{th}^{(1)}$. Beyond this value the system operates in the bimode state where the buildup time for mode 2 exhibits overshoot behavior for values of J slightly larger than $\tilde{J}_{th}^{(2)}$. For both wavelengths, the trend is decreasing and values as low as 30 ps are obtained for a value of $J = 6J_{th}^{(1)}$.

ACKNOWLEDGMENTS

The authors are much indebted to Dr. F. Dessenne from IEMN, University Lille 1, for his generous help. Moreover, S. Lamari and A. Hamadou are grateful to the Algerian Ministry of Higher Education for a research grant.

[1]J. Faist, F. Capasso, D. L. Sivco, C. Sirtori, A. L. Hutchinson, and A. Y. Cho, Science **264**, 553 (1994).
[2]M. W. Sigrist, *Air Monitoring by Spectroscopic Techniques*. (Wiley, New York, 1994).
[3]M. A. Belkin, F. Capasso, F. Xie, A. Belyanin, M. Fischer, A. Wittmann, and J. Faist, Appl. Phys. Lett. **92**, 201101 (2008); K. Vijayraghavan, Y. Jiang, M. Jang, A. Jiang, K. Choutagunta, A. Vizbaras, F. Demmerle, G. Boehm, M. C. Amann, and M. A. Belkin, Nat. Commun. **3021**, 1 (2013).
[4]Q. Y. Lu, N. Bandyopadhyay, S. Slivken, Y. Bai, and M. Razeghi, Appl. Phys. Lett. **99**, 131106 (2011); **101**, 251121 (2012); Opt. Express **21**, 968 (2013); Appl. Phys. Lett. **103**, 011101 (2013); Proc. SPIE **8631**, 863108 (2013).
[5]C. Jirauschek, A. Matyas, P. Lugli, and M.-C. Amann, Opt. Express **21**, 6180 (2013).
[6]C. Sirtori, A. Tredicucci, F. Capasso, J. Faist, D. L. Sivco, A. L. Hutchinson, and A. Y. Cho, Opt. Lett. **23**, 463 (1998).
[7]A. Tredicucci, C. Gmachl, F. Capasso, D. L. Sivco, A. L. Hutchinson, and A. Y. Cho, Nature **396**, 350 (1998).
[8]A. Friedrich, G. Scarpa, G. Boehm, and M.-C. Amann, Electron. Lett. **41**, 529 (2005).
[9]A. Straub, T. S. Mosely, C. Gmachl, R. Colombelli, M. Troccoli, F. Capasso, D. L. Sivco, and A. Y. Cho, Appl. Phys. Lett. **80**, 2845 (2002).
[10]M. Geiser, C. Pflügl, A. Belyanin, Q.-J. Wang, N.Yu, T. Edamura, M. Yamanishi, H. Kan, M. Fischer, A. Wittmann, J. Faist, and F. Capasso, Opt. Express **18**, 9900 (2010).
[11]C. Gmachl, D. L. Sivco, J. N. Baillargeon, A. L. Hutchinson, F. Capasso, and A. Y. Cho, Appl. Phys. Lett. **79**, 572 (2001).
[12]K. J. Franz, S. Menzel, A. J. Hoffman, D. Wasserman, J. W. Cockburn, and C. Gmachl, Nature Photon. **3**, 50 (2009).
[13]A. Hamadou, S. Lamari, and J.-L. Thobel, J. Appl. Phys. **105**, 093116 (2009).
[14]Y. Petitjean, F. Destic, S. Barbieri, C. Sirtori, and J.-C. Mollier, Proc. SPIE **7763**, 776306 (2010).
[15]A. Hamadou, J.-L. Thobel, and S. Lamari, Opt. Commun. **305**, 147 (2013).
[16]D. Hofstetter, M. Beck, T. Aellen, and J. Faist, Appl. Phys. Lett. **78**, 396 (2001).
[17]D. Hofstetter, M. Beck, T. Aellen, J. Faist, U. Oesterle, M. Ilegems, E. Gini, and H. Melchior, Appl. Phys. Lett. **78**, 1964 (2001).
[18]J. Faist, D. Hofstetter, M. Beck, T. Aellen, M. Rochat, and S. Blaser, IEEE J. Quant. Electron. **38**, 533 (2002).
[19]J. Faist, M. Beck, T. Aellen, and E. Gini, Appl. Phys. Lett. **78**, 147 (2001).
[20]H. C. Liu and F. Capasso, *Intersubband Transitions in Quantum Wells: Physics and Device Applications I* (Academic Press, 2000), vol. 62, chap. 1, p. 99.
[21]V. D. Jovanović, S. Höfling, D. Indjin, N. Vukmirović, Z. Ikonić, P. Harrison, J. P. Reithmaier, and A. Forchel, J. Appl. Phys. **99**, 103106 (2006).
[22]M. Yamanishi, T. Edamura, K. Fujita, N. Akikusa, and H. Kan, IEEE J. Quant. Electron. **44**, 12 (2008).
[23]R. C. Iotti and F. Rossi, Rep. Prog. Phys. **68**, 2533 (2005).
[24]M. Troccoli, G. Scamarcio, V. Spagnolo, A. Tredicucci, C. Gmachl, F. Capasso, D. L. Sivco, A. Y. Cho, and M. Striccoli, Appl. Phys. Lett. **77**, 1088 (2000).